Rock and Soil Mechanics

Volume 43 | Issue 1 Article 4

3-23-2022

Establishment of constitutive relation of shear deformation for irregular joints in sandstone

Tan CHENG
School of Energy Science and Engineering, Henan Polytechnic University, Jiaozuo, Henan 454000, China

Bao-hua GUO
The Collaborative Innovation Center of Coal Safety Production of Henan Province, Henan Polytechnic University, Jiaozuo, Henan 454000, China, guobaohua@139.com

Jie-hao SUN
School of Energy Science and Engineering, Henan Polytechnic University, Jiaozuo, Henan 454000, China

Shi-xuan TIAN
School of Energy Science and Engineering, Henan Polytechnic University, Jiaozuo, Henan 454000, China

See next page for additional authors

Custom Citation

CHENG Tan, GUO Bao-hua, SUN Jie-hao, TIAN Shi-xuan, SUN Chong-xuan, CHEN Yan, . Establishment of constitutive relation of shear deformation for irregular joints in sandstone[J]. Rock and Soil Mechanics, 2022, 43(1): 51-64.

Establishment of constitutive relation of shear deformation for irregular joints in sandstone

Authors

Tan CHENG, Bao-hua GUO, Jie-hao SUN, Shi-xuan TIAN, Chong-xuan SUN, and Yan CHEN

Rock and Soil Mechanics 2022 43(1): 51−64 ISSN 1000−7598
https: //doi.org/10.16285/j.rsm.2021.5832 rocksoilmech.researchcommons.org/journal

Establishment of constitutive relation of shear deformation for irregular joints in sandstone

CHENG Tan[1], GUO Bao-hua[1, 2], SUN Jie-hao[1], TIAN Shi-xuan[1], SUN Chong-xuan[1], CHEN Yan[1]

1. School of Energy Science and Engineering, Henan Polytechnic University, Jiaozuo, Henan 454000, China

2. The Collaborative Innovation Center of Coal Safety Production of Henan Province, Henan Polytechnic University, Jiaozuo, Henan 454000, China

Abstract: The shear deformation of rock joints is significant for the safety and stability of rock engineering. In order to study the constitutive relation of shear deformation in jointed rock mass under a normal stress, the direct shear tests under different normal stresses were carried out on the sandstone specimens with irregular joints using the RDS-200 rock direct shear test system. Based on the shear stress−deformation curve of the jointed rock, it can be divided into four stages including pre-peak compaction stage, linear stage, yield stage and post-peak softening stage. The post-peak softening stage can be further divided into three types including platform type, gradual decline type and drop type based on the decreasing magnitude and rate of shear stress at the post-peak period. The shear deformation constitutive model of the sandstone with irregular joints was established using piecewise function based on the shear deformation characteristics at different stages. Compared with the existing constitutive models, the new proposed shear deformation constitutive model of the jointed rock mass has a much higher fitting accuracy for the experimental results, which can better describe the deformation characteristics of the jointed rock in the whole shear process. The shear stress−shear displacement curve of irregular joints with different roughness coefficients under different normal stresses can be predicted after determining the relevant model parameters in the corresponding empirical formula after some direct shear tests. The research is practical for understanding the shear deformation of joints in rocks by numerical simulation and the safety evaluation of engineering.

Keywords: rock mechanics; rock joints; shear deformation; constitutive relation; empirical formula

1 Introduction

The widely distributed joints in rocks can easily affect the strength and deformation behavior of rock masses. The study of the deformation characteristics of joints is of great significance to improve the safety and stability of rock engineering. The shear failure is the main failure mode for rock joints. Understanding the shear deformation characteristics in the shear failure process of rock joint is helpful to predict the shear failure of rock joints and estimate the mechanical state of rock joints after failure. Therefore, the shear deformation constitutive model of rock joints has always become the hot research issue in the field of rock mechanics. Since the 1960s, based on a series of experimental and theoretical analysis, many researchers have established some shear displacement constitutive models for rock joints which can describe the relationship of shear stress−displacement curve of rock joints.

Goodman et al.[1−2] proposed the joint element modeling method and established a linear elastic constitutive model at the pre-peak of the joint, which was similar to the generalized Hook's law by analyzing the relationship between the macroscopic nonlinear deformation of the joint and the nonlinear failure of the micro-protrusion at the joint contact. Bandis et al.[3] summarized the direct shear experimental results of different types of rock joints and established the hyperbolic functions to describe the shear deformation behavior of joints. Desai et al.[4] established an isotropic hardening constitutive model of joint based on plasticity theory. All these studies mainly focused on the pre-peak part of the joint shear stress−displacement curve, but rarely involved the post-peak of the shear stress−displacement curve.

Saeb et al.[5] studied the entire shear deformation curve of rock joints, using linear functions to describe the shear stress−shear displacement relationship in the pre-peak stage, post-peak softening stage, and residual stage, respectively. It was a general extension of the Goodman's model [2]. A large number of direct shear tests have implied that the joint shear stress−displacement curve had a nonlinear stage before and after the peak[6−7]. The linear function model proposed by Saeb et al [5] can not describe the nonlinear behavior of joint shear deformation before and after the peak. Based on the results of shear tests of rock joints under constant normal load, Amadei et al.[8] proposed the hyperbolic

Received: 3 June 2021 Revised: 9 September 2021
This work was supported by the National Natural Science Foundation of China (51904092, 52104127), the Fundamental Research Funds for the Universities of Henan Province (NSFRF180336, NSFRF210303), the Natural Science Foundation of Henan (202300410183) and the Key Scientific Research Projects of Colleges and Universities in Henan Province (21A440003).
First author: CHENG Tan, male, born in 1993,,PhD candidate, focusing on rock fracture deformation and seepage. E-mail: 451953767@qq.com
Corresponding author: GUO Bao-hua, male, born in 1979, PhD, Professor, research interests: rock fracture deformation and seepage. E-mail:guobaohua@139.com

and linear functions to describe the relationship between shear stress and shear displacement at the pre-peak and post-peak of joint, respectively. Simon[9] believed that the exponential function can better describe the nonlinear relationship between shear stress and shear displacement, and proposed a complete stress−displacement surface (CSDS) model. However, it had no explicit solution, and the iterative calculation was required to obtain the model parameters, making it not convenient to be applied in actual engineering analysis[6]. Grasselli et al.[10] conducted direct shear tests on 7 types of rock tensile joints under constant normal load conditions, and proposed the hyperbolic function to fit the post-peak part of the shear stress−deformation curve, but the linear function was used to describe the pre-peak part of the shear stress-deformation curve, which was inconsistent with the results of some direct shear tests [11−12]. Tang et al.[6,13−14] proposed the hardening-softening shear displacement constitutive model of the rock with a through joint, the shear displacement constitutive model of non-consecutive joint rock mass, and the normalized displacement softening model of joint at the post-peak, but these constitutive models did not determine the quantitative relationship of constitutive model parameters, normal stress and joint roughness. Based on the statistical damage theory and the macroscopic and microscopic deformation characteristics of rock joints, Xie[15−17] and Lin[18] proposed the damage constitutive models to describe the complete shear deformation curve of joints.

After establishing the quantitative relationship between the constitutive model parameters (e.g., pre-peak shear stiffness, peak shear displacement, peak shear stress and residual strength) and the physical and mechanical parameters of rock joints or test condition parameters, the shear deformation constitutive model of rock joints can be used to predict the shear stress−displacement curve of rock joints under different normal stress conditions. At present, the quantitative relationship of pre-peak shear stiffness, peak shear displacement and peak shear stress at different rock joint constants or test condition parameters are widely studied, while the residual strength is rarely studied due to the large discreteness.

In terms of pre-peak shear stiffness, Nassir et al. [19] established the calculation formula of stiffness parameters of jointed rock mass through theoretical analysis. Kulhawy[20] studied the joint shear deformation characteristics before shear failure, and established the relationship between shear stiffness and normal stress. Bandis[3] modified the Kulhawy's equation by introducing the function τ/τ_p (τ was the shear stress, τ_p was the peak shear stress), making the empirical formula can represent the variation of shear stiffness to some extent. Qi et al.[21] modified the shear stiffness empirical formula proposed by Bandis based on shear tests and numerical analysis, which was consistent to the actual engineering.

In terms of peak shear stress, Patton[22] used a single dentate joint specimen to study the influence of joint morphology on the mechanical properties of joints. Based on the climbing effect and tooth cutting effect, the two-line model was proposed to describe the peak shear stress of joints, which was similar to the Mohr-Coulomb criterion. Based on a large number of rock joint shear tests, Barton[23] introduced the joint roughness coefficient JRC (joint roughness coefficient), and proposed the peak shear strength criterion for irregular rock joints—JRC-JCS(joint compressive strength) model. Grasselli et al.[24] studied the relationship between the effective apparent inclination angle and the potential contact area ratio of the joint micro-bumps, and proposed a three-dimensional topography parameter that can reflect the shear direction and the effective shear area. On this basis, the peak shear stress model was established. Xia et al.[25] proposed a new peak shear stress formula based on the three-dimensional topography parameters of the Grasselli's model and the variation law of the joint dilatancy angle. Jin et al.[26] used the artificial joint specimens to conduct direct shear tests under constant normal stress, and established a shear strength model considering the three-dimensional topography parameters and tensile strength parameters. Fan et al.[27] studied the impacts of JRC, JCS and normal stress on the peak shear strength of joints, and proposed a peak shear strength model suitable for soft-hard joints.

In terms of peak shear displacement, Barton et al. [28] conducted shear tests on joint specimens with different lengths and found that the shear displacement was about 1% of the joint specimen length L along the shear direction when the joint reaches the peak shear stress. Wibowo[29] considered the influence of the normal stress on the peak shear displacement and proposed a linear formula to describe the relationship between the joint peak shear displacement and the normal stress. Barton[30] analyzed the test data provided by Bandis and found that the ratio of peak shear displacement to joint length was related to the joint roughness coefficient JRC, and proposed an empirical formula of joint peak shear displacement considering joint length and roughness. Asadollahi et al.[31] analyzed a large set of joint shear test data in literatures, and found that the peak shear displacement of joints was affected by the combined effect of normal stress, joint length and joint roughness. Based on the theoretical analysis, it showed that the peak shear displacement was positively correlated with stress, and was negatively correlated with the roughness coefficient JRC. Furthermore, an empirical formula for peak shear displacement considering normal stress, joint length and joint

roughness was proposed. Xia et al.[32] verified that the peak shear displacement was positively correlated with the normal stress and negatively correlated with the roughness coefficient JRC through indoor direct shear tests. An empirical formula for the peak shear displacement of a regular tooth joint was established. Ban et al.[33] used the equivalent dilatancy angle to replace the undulation angle in the peak shear displacement empirical formula of regular tooth-shaped joints proposed by Xia et al.[32], and obtained the empirical formula suitable for the peak shear displacement of irregular joints. The dilatancy angle in the joint peak shear displacement empirical formula proposed by Asadollahi[31] and Ban[33] was based on the two-dimensional roughness coefficient JRC, which was difficult to fully reflect the realistic three-dimensional morphological characteristics of the joints.

In summary, the existing rock joint shear deformation constitutive model still has some shortcomings in the description of the deformation characteristics of the shear stress−displacement curve at each stage, and the relevant parameters in the constitutive model need to be determined based on the direct shear tests. It is inconvenient to predict and estimate the shear deformation characteristics of rock joints in actual engineering. In this paper, the direct shear tests on irregular sandstone joints under different normal stresses were carried out to analyze the segmental deformation characteristics of the shear stress−displacement curves of rock joints under different normal stresses. The relationship between parameters in the description functions of each stage, the basic physical and mechanical parameters, normal stress and/or joint morphology were established. The constitutive model that can describe the entire shear deformation curve of irregular rock joints under different normal stresses was proposed to compare with the existing constitutive models of rock joints. The constitutive model was used to predict the shear stress−displacement curve of irregular rock joints under different normal stresses, which was helpful to the numerical analysis and engineering estimation of the stability of jointed rock masses.

2 Experiments

2.1 Preparation of specimens

The sandstone taken from a quarry in Sichuan province was composed of quartz, potash feldspar and albite. The particle size was about 0.10−0.25 mm. First of all, after drilling, sawing and grinding, the sandstone was made into ten standard cylindrical specimens of Φ50 mm×100 mm (5 specimens were used for uniaxial compression tests, another 5 specimens were used for triaxial compression tests), and 5 intact specimens of Φ50 mm×25 mm were used for Brazil split test, according to the related standards. The self-made specimen splitting mold[34] was used to make the tensile joints near the axial midpoint for 11 cylindrical sandstone specimens of Φ50 mm×100 mm. These 11 sandstone joint specimens were used for direct shear test and the manufacturing process is shown in Fig. 1.

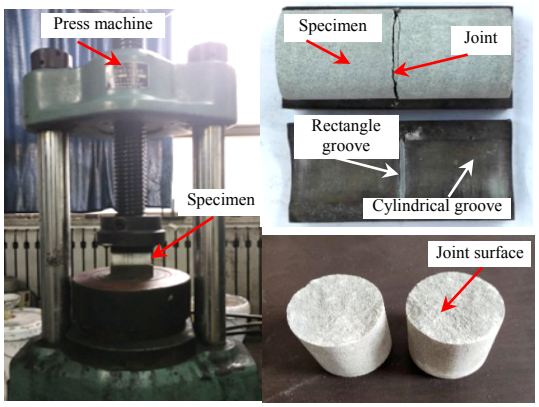

Fig. 1 Preparation sequence of the jointed rock mass

The complete standard cylindrical specimens were used for the uniaxial, triaxial and Brazilian splitting tests on the RMT-150B rock mechanics servo testing machine developed by the Wuhan Institute of Rock and Soil Mechanics, Chinese Academy of Sciences. Each test was repeated for 5 times to obtain the basic physical and mechanical parameters of sandstone specimens including compressive strength σ_c, tensile strength σ_t, cohesion c, internal friction angle φ_0, Poisson's ratio μ and elastic modulus E, as shown in Table 1. The basic friction angle φ_b of rock joints was tested by the tilt test of standard cylindrical specimens[35], which was also listed in Table 1.

Table 1 Basic mechanical properties of sandstone

Rock type	σ_c /MPa	σ_t /MPa	c /MPa	φ_0 /(°)	μ	E /GPa	φ_b /(°)
Sandstone	83.48	4.15	15.8	33.6	0.211	16.90	32.12

2.2 Topography parameters of rock joint

The Tianyuan OKIO-400 three-dimensional scanner[34] was used to obtain the three-dimensional coordinate data of the joint surface. The three-dimensional topography parameters of the joint surface were obtained by analyzing the scanning data in the analysis software. The joint topography and the setting method of profiles are shown in Fig.2. The Tianyuan OKIO-400 three-dimensional scanner uses a global error control module to control the scanning accuracy of joint topography. The average accuracy is 0.02−0.03 mm, the average point distance is 0.31−0.15 mm, and the maximum coverage scanning area is 400 mm×300 mm.

In addition, the roughness coefficient JRC of the joint can be determined by calculating the root mean square of slope Z_2 of each profile (Fig. 2(b)). The

calculation formula of Z_2 is written as follows:

$$Z_2 = \left[\frac{1}{(l-1)(\Delta x)^2} \sum_{i=1}^{l-1} (y_{i+1} - y_i)^2 \right]^{1/2} \quad (1)$$

where y_i is the height coordinate of the joint surface profile of sampling point i; l is the number of data points; Δx is the interval of data points; and subscript i is the natural number.

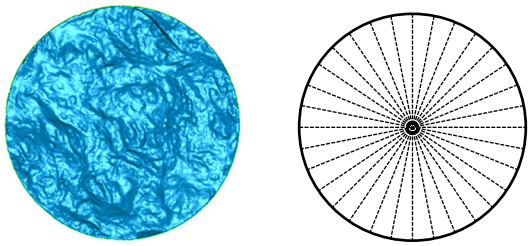

(a) Scanning morphology of joint surface (b) Layout of profiles

Fig. 2 Scanned morphology of joint surface and layout of profiles

Then, substituting the Z_{2i} of each two-dimensional profile line into the following formula[36] to calculate the roughness coefficient JRC_i of the i-th profile line of the joint.

$$JRC_i = 32.69 + 32.98 \lg Z_{2i} \quad (2)$$

where Z_{2i} is the root mean square of slope of the i-th profile.

Finally, the weighted average value of JRC_i for all two-dimensional profiles is calculated to obtain the joint roughness coefficient JRC that can reflect the three-dimensional topography of the joint surface.

$$JRC = \frac{1}{w} \sum_{i=1}^{w} JRC_i \quad (3)$$

where w is the total number of two-dimensional profiles, and 16 profiles are set in this paper.

2.3 Experimental apparatus

The direct shear test was completed with the RDS-200 rock direct shear apparatus[34] produced by the GCTS company. The overall appearance and schematic of the equipment are shown in Figs. 3 and 4, respectively.

The electro-hydraulic servo control system is used in the direct shear instrument to control the loads in the normal and shear directions. The maximum loads in the shear and the normal loading actuators are 10 t and 5 t, respectively, with an accuracy of 0.01 kN. The maximum strokes in the shear and the normal directions are 25 and 24 mm, respectively, with an accuracy of 0.001 mm. The inside part of the shearing mechanism is composed of upper and lower steel rings. The inner diameter of the ring is about 150 mm. The upper and lower rings do not touch each other. When the specimen is sealed, it is separated by two detachable semicircular metal backing rings, which are removed during the test. The upper and lower shear rings are put into the upper and lower shear boxes. The lower shear box is fixed on the black frame platform, and the upper shear box is seamlessly linked with the shear actuator through the pin. The shear load is transmitted to the upper shear box through the shear actuator and the pin, and the direction of the shear load is parallel to the joints of specimens.

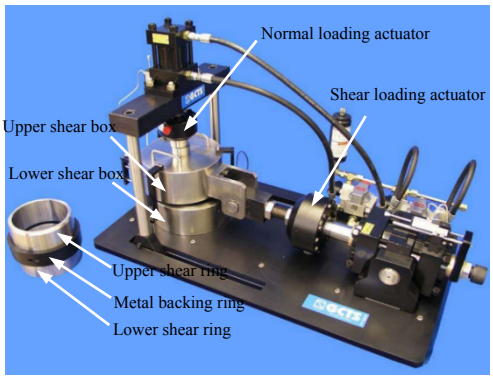

Fig. 3 RDS-200 direct shear test system

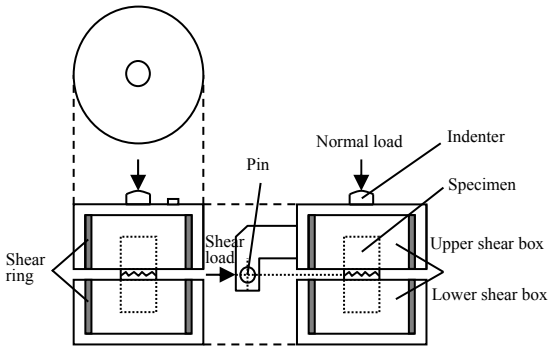

Fig. 4 Schematic diagram of shear box

The direct shear test process is controlled by a computer. The control software is a computer aided testing software standard (CATS), which can realize three boundary conditions including constant normal load (CNL), constant normal stiffness (CNS), constant normal displacement (CNV), and multiple control methods of combined CNL, CNS and CNV. The test process is automatically controlled by CATS software, which can output graphics such as shear and normal stress−displacement curves, and displays the test process in real time. The test data is monitored by the sensor and is input into the computer. After the test, the data can be output to a text file, which can be imported into Excel and other office software for processing.

2.4 Experimental scheme

The direct shear test was carried out in the CNL control mode, and the initial values of the normal stress were 3, 6, 9, 12, 15, 18, 21, and 24 MPa. The detailed experimental processes were as follows: (1) the normal stress was applied to the design value according to the load control mode; (2) the tangential load was applied by displacement control, with a shear rate of 1 mm/min; and (3) the direct shear process was

controlled by the servo system to keep the normal stress constant, and the shear test stopped at the shear displacement of 8 mm. During the shear test, parameters such as normal stress, normal displacement, shear stress, and shear displacement were recorded.

3 Shear tests results and analysis

3.1 Shear stress−displacement curve

The shear stress−displacement curves of sandstone joints are shown in Fig. 5. It can be seen from Figs. 5(a) − 5(c) that the shear stress−displacement curves present different shape characteristics under different normal stresses. The whole curve of rock joint shear stress−displacement can be divided into pre-peak compaction stage, linear stage, yield stage and post-peak softening stage. The decrease rate of shear stress increases with the increase of normal stress in the post-peak softening stage. Therefore, the shear stress−displacement curves of rock joints at the post-peak stage can be divided into plateau type, slow drop type and rapid drop type, as shown in Figs. 5(d)−5(f).

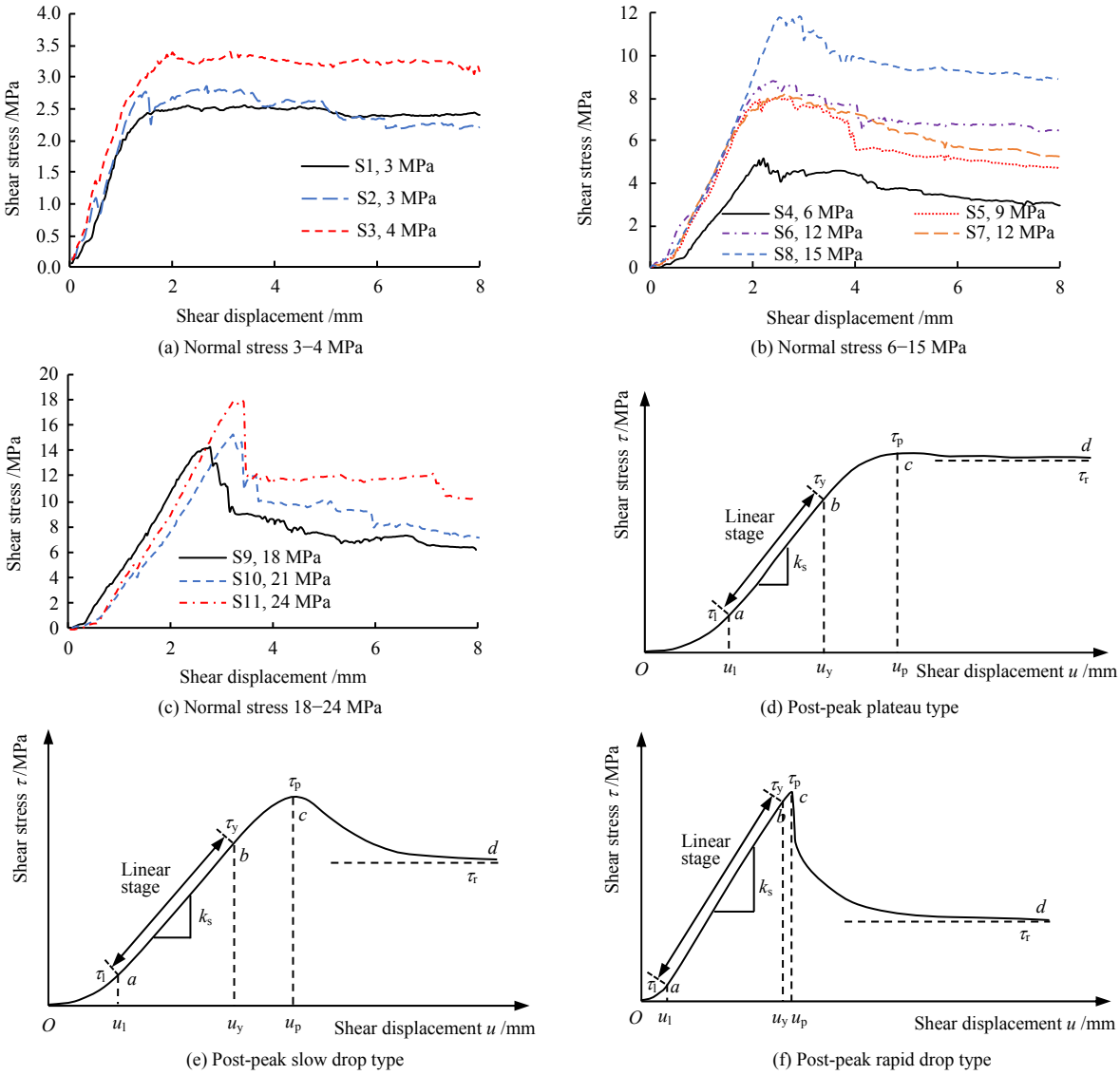

(a) Normal stress 3−4 MPa

(b) Normal stress 6−15 MPa

(c) Normal stress 18−24 MPa

(d) Post-peak plateau type

(e) Post-peak slow drop type

(f) Post-peak rapid drop type

Fig. 5 Shear stress−displacement curves under different normal stresses

In Figs. 5(d)−5(f), k_s is the pre-peak shear stiffness; u_l and τ_l are the shear displacement and shear stress corresponding to the starting point of the linear section at the pre-peak stage of the shear stress−displacement curve; u_y and τ_y are the shear displacement and shear stress at the starting point of the pre-peak yield phase, respectively; u_p and τ_p are the peak shear displacement and peak shear stress; and τ_r is the residual shear strength, which can be calculated by using the shear stress corresponding to the horizontal asymptotic line of the post-peak deformation curve. The variation characteristics of the shear stress−displacement curve at each stage are as follows: (1) Compaction stage, see the section *oa* in Figs. 5(d)−5(f). Due to the incomplete contact between the two joint surfaces in the initial state, the contact area and contact pressure of the joint protrusions increase with the increase of the shear displacement, and the shear stress τ increases nonlinearly

and rapidly with the increase of the shear displacement u. (2) Linear stage, see section *ab* in Figs. 5(d)−5(f). Potentially accessible joint surface bulges are close to full contact. When the shear displacement increases, the contact stress of the protrusions continues to increase in the non-failure state of the contact protrusions. From the macroscopic point of view, the joint shear stress increases linearly with the increase of the shear displacement. (3) Yield stage, see section *bc* in Figs. 5(d)−5(f). Partly contacted bulges begin to wear or shear, resulting in the increase in the shear displacement. The damaged joint surface bulges can not continue to provide shear resistance, and the shear resistance provided by the new contacted bulges is still greater than that of the loss of shear resistance due to bulge failure. The joint shear stress decreases with the increase of shear displacement, until the shear resistance provided by the new contact bulge is equal to the loss in the shear resistance due to the damage of the original contact bulge, and the shear capacity of the joints reaches to the peak. (4) Post-peak stage, see *cd* section in Figs.5(d)−5(f). The shear stress−displacement curves of rock joints in the post-peak stage can be divided into plateau type, slow drop type and rapid drop type.

The shear stress−displacement curve of the rock joint at the post-peak plateau is shown in Fig.5(d). The shear stress does not decrease significantly after the peak. This type of shear stress−displacement curve occurs at the low initial normal stress condition (e.g., 3 MPa and 4 MPa). The shear stress−displacement curve of the rock joint at the post-peak slow drop type is shown in Fig. 5(e). The shear stress decreases slowly after the peak, and the decrease rate gradually reduces until the shear stress tends to the residual shear strength. This type of shear stress−displacement curve occurs in the medium initial normal stress (6−15 MPa). The shear stress−displacement curve of the rock joint at the post-peak drop period is shown in Fig. 5(f). The shear stress drops rapidly after the peak, and then it decreases slowly till the residual strength. This type of post-peak drop curve of shear stress−displacement occurs at a much higher initial normal stress (18−24 MPa).

The aforementioned shear stress−displacement curve is formed by the loss of shear resistance of the contacted bulges due to damage. When the initial normal stress is low, the contact state of joint bulges at the post-peak changes, but there is no obvious failure. Some joint bulges lose shear resistance when they are no longer in contact, other new contacted bulges provide roughly equivalent shear resistance, so that the macroscopic shear stress of rock joints is not significantly reduced. When the initial normal stress is at medium level, the post-peak contacted bulges continue to lose shear resistance after the continuous failure. The shear resistance provided by the new contacted bulges is less than the shear resistance lost due to the damage of the initial contact bulges, but the difference is not very significant, leading to a macroscopically gradual reduction in the shear stress of rock joints. When the initial normal stress is high, the shear resistance is zero due to the simultaneous failure of a large number of contacted bulges at the post-peak. The shear resistance provided by the instantaneous new contacted bulges is much smaller than the loss value due to the massive damage of the contacted bulges. Therefore, the drop of shear stress of rock joints appears macroscopically. Thereafter, as the shear displacement increases, the contacted bulges lose shear resistance due to continuous failure; while the shear resistance provided by the new contacted bulges is less than the shear resistance lost due to the damage of the initial contacted bulges, but the difference is not large, making the shear stress of rock joints gradually decrease macroscopically.

3.2 Shear stress−displacement curve fitting equations

During the compaction stage, the shear deformation of rock joints is mainly characterized as the adjustment of the bulge contact state, and the shear stress increment is relatively small. This paper does not consider its description and prediction methods. By analyzing the characteristics of the linear stage, the yield stage at the pre-peak and the post-peak softening stage of the typical shear stress−displacement curve, the description method of the curve at each stage is determined as follows.

(1) Linear stage before peak. The shear stress τ increases almost linearly with the increase of the shear displacement u, and the increase rate is the shear stiffness k_s, which can be described by a linear model [12−13,17].

$$\tau = k_s u \tag{4}$$

Due to the existence of the pre-peak compaction stage, the starting point of the pre-peak linear stage is not the point where the shear displacement is zero, and the shear displacement u in Eq. (4) needs to be corrected. The fitted straight line in the pre-peak linear stage intersects with the horizontal axis at a point (u_i, 0). The x-coordinate u_i of the starting point of the pre-peak linear stage can be calculated by the following equation.

$$u_i = u_y - \frac{\tau_y}{k_s} \tag{5}$$

Substituting Eq. (5) into Eq. (4), the shear stress at the pre-peak linear stage is obtained as follows:

$$\tau = k_s \left[u - \left(u_y - \frac{\tau_y}{k_s} \right) \right], \ u_i < u \leqslant u_y \tag{6}$$

(2) Pre-peak yield stage. The shear stress curve

passes the starting point (u_y, τ_y) and the peak point (u_p, τ_p) of the yield stage. The curve is concave upward, and the shear stress τ increases at a decelerating rate as the shear displacement u increases. Thus, a nonlinear function can be used to describe the shear stress at this stage.

$$\tau = \frac{u-u_y}{r\left(u-u_y\right)^n + z} + \tau_y,\ u_y < u \leqslant u_p \tag{7}$$

where r, n, and z are fitting parameters, which are related to the shape of the shear stress−displacement curve.

It is assumed that the peak point (u_p, τ_p) of the shear stress−displacement curve satisfies the following relationship[6, 15]:

$$\left.\begin{aligned} \tau\big|_{u=u_p} &= \tau_p \\ \frac{\mathrm{d}\tau}{\mathrm{d}u}\bigg|_{u=u_p} &= 0 \end{aligned}\right\} \tag{8}$$

From Eqs. (7) and (8), r and z can be rewritten as

$$r = \frac{1}{n\left(\tau_p-\tau_y\right)\left(u_p-u_y\right)^{n-1}} \tag{9}$$

$$z = \frac{(n-1)\left(u_p-u_y\right)}{n\left(\tau_p-\tau_y\right)} \tag{10}$$

Substituting Eqs. (9) and (10) into Eq. (7), the shear stress at the pre-peak yield stage is written as

$$\tau = \frac{n\left(u-u_y\right)\left(\tau_p-\tau_y\right)\left(u_p-u_y\right)^{n-1}}{\left(u-u_y\right)^n + (n-1)\left(u_p-u_y\right)^n} + \tau_y,\ u_y < u \leqslant u_p \tag{11}$$

The influence of parameter n on the pre-peak yield stage is shown in Fig. 6. It can be seen from Fig. 6 that the parameter n controls the curvature of the curve in the pre-peak yield stage. When the parameter n is small, the curvature of the curve is large. With the increase of the parameter n, the curvature of the curve becomes much smaller and the shear stress−displacement curve gradually becomes a straight line. Then it transfers from deceleration yielding to constant yielding.

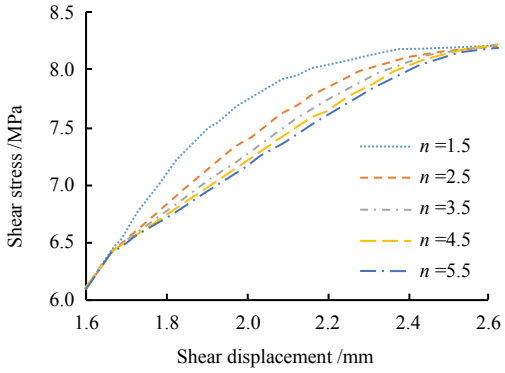

Fig. 6 Effect of parameters *n* on constitutive relation

(3) Post-peak softening stage. In the post-peak stage, as the shear displacement increases, the joint bulge is gradually damaged by abrasion, the shear stress gradually decreases until trends to the residual shear strength. The plateau type curve at the post-peak is a specific example where the joint bulge wear and damage are not obvious. The curve in the post-peak softening stage is concave downward, the reduction rate of the shear stress gradually decreases and passes through the peak point (u_p, τ_p). The nonlinear function is used to describe the shear stress at this stage.

$$\tau = \left(\tau_p-\tau_r\right)\exp\left[-t\left(u-u_p\right)^m\right] + \tau_r,\ u > u_p \tag{12}$$

where t and m are fitting parameters, $t>0$, $m>0$.

It can be seen from Eq. (12) that τ_p is the limit value of shear stress when the shear displacement u tends to u_p, and τ_r is the limit value of shear stress when the shear displacement u tends to infinity. The influences of the parameters t and m on the shape of the curve are shown in Fig. 7.

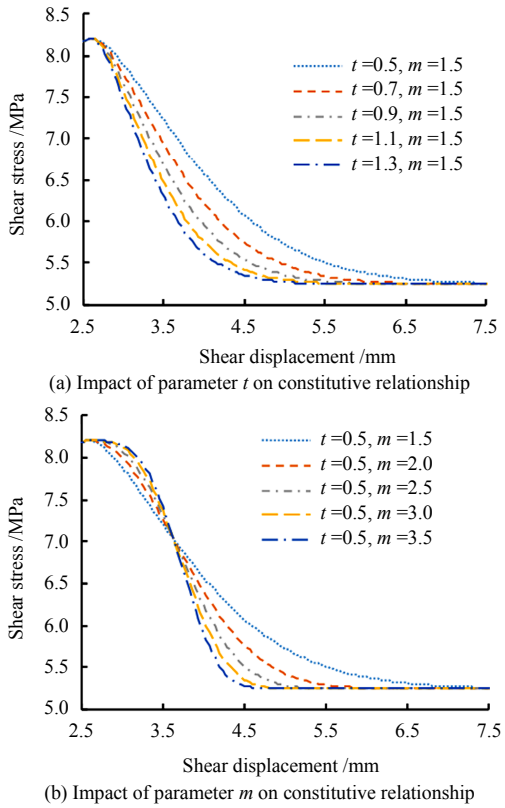

Fig. 7 Effect of parameters *t* and *m* on constitutive relation

It can be seen from Fig. 7(a) that the larger the parameter t, the greater the reduction rate of shear stress in the post-peak softening stage, and the faster the shear stress tends to the residual strength. It can be seen from Fig. 7(b) that all curves intersect at the position 1 mm after the peak displacement when t is a constant. Under the same shear displacement, the shear stress before the intersection point increases as the value of m increases, and the shear stress after the

intersection point decreases as the value of m increases. It can also be seen from Fig. 7(b) that the larger the parameter m, the wider the platform at both ends of the curve in the post-peak softening stage, the greater the reduction rate of the shear stress curve between the two platforms. The greater of the initial shear displacement where the shear stress starts to decrease rapidly, the smaller the shear displacement to reach the residual shear stress. Therefore, the changes in the values of the parameters t and m can describe the different curve shapes at the post-peak softening stage.

The following piecewise function can be used to describe the whole shear stress−displacement curve of rock joints.

$$\tau=\begin{cases}k_{\mathrm{s}}\left[u-\left(u_{\mathrm{y}}-\dfrac{\tau_{\mathrm{y}}}{k_{\mathrm{s}}}\right)\right], u_{\mathrm{i}}<u\leqslant u_{\mathrm{y}}\\ \dfrac{n\left(u-u_{\mathrm{y}}\right)\left(\tau_{\mathrm{p}}-\tau_{\mathrm{y}}\right)\left(u_{\mathrm{p}}-u_{\mathrm{y}}\right)^{n-1}}{\left(u-u_{\mathrm{y}}\right)^{n}+\left(n-1\right)\left(u_{\mathrm{p}}-u_{\mathrm{y}}\right)^{n}}+\tau_{\mathrm{y}}, u_{\mathrm{y}}<u\leqslant u_{\mathrm{p}}\\ \left(\tau_{\mathrm{p}}-\tau_{\mathrm{r}}\right)\exp\left[-t\left(u-u_{\mathrm{p}}\right)^{m}\right]+\tau_{\mathrm{r}}, u_{\mathrm{p}}<u\end{cases} \tag{13}$$

3.3 Shear stress−displacement curve fitting effect

The steps for fitting the shear stress−displacement curve are as follows:

(1) The relevant parameters k_{s}, u_{y}, u_{p}, τ_{y}, and τ_{p} in Eq. (13) can be directly obtained from the direct shear test, see Table 2 for much details. σ_{n} is the normal stress, and R_{s} is the profile area ratio. The default value of the normal stress of the specimen S3 is 6 MPa. When the normal stress value is input, it is mistakenly set to 4 MPa, which is also listed in Table 2.

(2) The experimental values of parameters k_{s}, u_{y}, u_{p}, τ_{y}, and τ_{p} are substituted into Eqs. (11) and (12), respectively, to fit the direct shear test data and obtain the values of parameters n, t, m and τ_{r}, see Table 2 for much details. Because the maximum shear displacement is set as a small value, some test curves at the post-peak stage do not obviously enter the residual stage, resulting in several negative values of fitting residual shear strength (S4, S10). Thus, the fitting of the shear stress at the post-peak stage is not performed.

(3) Substituting all model parameters into Eq. (13), the segmented function of the curve fitting for each group of test data can be obtained.

Table 2 Relevant parameters in the constitutive model

Specimen No.	σ_{n}/MPa	JRC	R_{s}	k_{s}/(MPa • mm^{-1})	τ_{i}/MPa	τ_{y}/MPa	τ_{p}/MPa	u_{i}/mm	u_{y}/mm	u_{p}/mm	τ_{r}/MPa	n	t	m
S1	3	6.64	1.027 8	2.25	0.45	2.11	2.54	0.40	1.14	1.52	2.39	2.944	0.07	7.264
S2	3	10.88	1.035 5	2.16	0.44	2.60	2.73	0.27	1.27	1.48	2.21	2.991	0.78	3.636
S3	4	8.54	1.029 9	2.47	0.71	2.69	3.38	0.33	1.14	2.00	3.22	4.130	0.79	6.539
S4	6	7.35	1.030 0	3.21	0.48	4.89	5.20	0.67	2.04	2.21	−36.91	3.669	1.81	0.646
S5	9	12.37	1.046 6	4.91	0.91	7.40	8.01	0.56	1.91	2.14	4.92	5.694	39.44	1.868
S6	12	7.59	1.031 6	4.51	0.61	8.24	8.82	0.34	2.03	2.40	6.66	10.733	58.65	1.417
S7	12	6.72	1.026 2	4.59	0.51	6.40	8.21	0.46	1.66	2.29	5.06	15.410	27.91	1.354
S8	15	8.13	1.030 5	5.63	2.12	11.57	11.88	0.76	2.44	2.53	9.12	16.442	71.22	1.277
S9	18	10.18	1.033 5	6.15	0.55	13.47	14.21	0.34	2.44	2.79	6.35	14.155	124.86	0.623
S10	21	7.87	1.032 6	5.70	1.79	14.06	15.26	0.81	2.96	3.23	−0.11	17.049	3.95	0.387
S11	24	8.70	1.033 8	6.65	0.59	16.37	18.05	0.59	2.97	3.39	11.60	26.336	382.01	0.232

In order to verify the rationality of Eq. (13), it is compared with Tang's model[13] and Xie's model[15−17]. Tang's model can be expressed as[13]

$$\tau=\begin{cases}k_{\mathrm{s}}u, 0<u\leqslant u_0\\ \tau_0+\dfrac{u-u_0}{\left(m_1+n_1u\right)^{a}}, u_0<u\leqslant u_{\mathrm{p}}\\ \tau_{\mathrm{r}}+\left(\tau_{\mathrm{p}}-\tau_{\mathrm{r}}\right)\left(\dfrac{u_{\mathrm{p}}}{u}\right)^{b}, u_{\mathrm{p}}<u\leqslant u_{\mathrm{r}}\\ \tau_{\mathrm{r}}, u_{\mathrm{r}}<u\end{cases} \tag{14}$$

where m_1, n_1, a, and b are all fitting parameters related to the shape of the shear stress−deformation curve. u_0 is the shear displacement of the starting point at the pre-peak yield stage; τ_0 is the shear stress of the starting point at the pre-peak yield stage; and u_{r} is the shear displacement at the starting point of the residual stage.

Xie's model can be written as[15−17]

$$\tau=\begin{cases}k_{\mathrm{s}}u, u<u_{\mathrm{s}}\\ \left(k_{\mathrm{s}}u-\tau_{\mathrm{r}}\right)\exp\left[-\left(\dfrac{u-u_{\mathrm{s}}}{u_0}\right)^{m_2}+\tau_{\mathrm{r}}\right], u_{\mathrm{s}}\leqslant u\end{cases} \tag{15}$$

$$m_2=\frac{k_{\mathrm{s}}\left(u_{\mathrm{p}}-u_{\mathrm{s}}\right)}{\left(k_{\mathrm{s}}u_{\mathrm{p}}-\tau_{\mathrm{r}}\right)\ln\left(\dfrac{k_{\mathrm{s}}u_{\mathrm{p}}-\tau_{\mathrm{r}}}{\tau_{\mathrm{p}}-\tau_{\mathrm{r}}}\right)};\quad u_0=\frac{u_{\mathrm{p}}-u_{\mathrm{s}}}{\left[\ln\left(\dfrac{k_{\mathrm{s}}u_{\mathrm{p}}-\tau_{\mathrm{r}}}{\tau_{\mathrm{p}}-\tau_{\mathrm{r}}}\right)\right]^{\frac{1}{m_3}}} \tag{16}$$

where u_{s} is the shear displacement of the starting point at the pre-peak yield stage; and m_2 is the distribution parameter of the function.

Three sets of calculation results are listed, representing the fitting effects of the shear stress−displacement curves of three post-peak deformation types. It includes the specimen S1 with an initial normal stress of 3 MPa (post-peak plateau type), specimen S6 with an initial normal stress of 12 MPa (post-peak slow drop type) and specimen S11 with an initial normal stress of 24 MPa (post-peak rapid drop type). Fig. 8 shows the comparison between the calculation and the experimental curves of the three models.

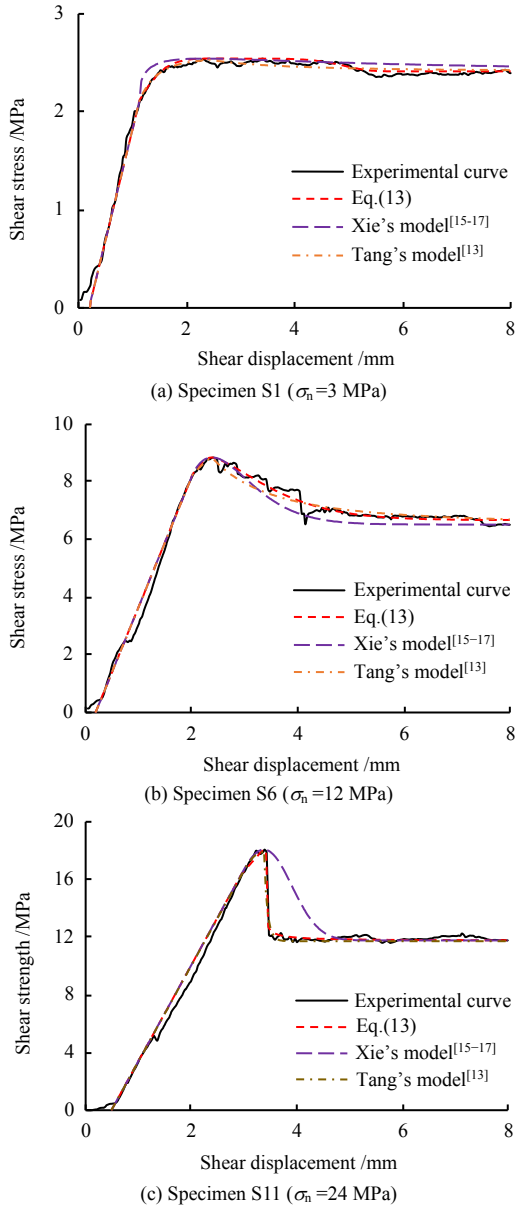

Fig. 8 Comparison of calculated and experimental shear stress-shear displacement curves

For the shear stress−displacement test curve with post-peak plateau under low normal stress, the fitting curves of Eq. (13), Tang's model[13] and Xie's model[15−17] are very close to the experimental curves in Fig. 8(a). But the fitting curve of Xie's model[15−17] is significantly higher than the test curve in the pre-peak yield stage, and it is also higher than the test curve in the second half of the plateau at the post-peak.

For the slow drop shear stress−displacement test curve at the post-peak under the medium normal stress, the fitting curves of Eq. (13) and Tang's model[13] are closer to the test curve in Fig. 8(b). The fitting curve of Xie's model[15−17] is significantly lower than the test curve in the post-peak softening stage.

For the shear stress−displacement test curve of the post-peak drop type under high normal stress, the fitting curves of Eq. (13) and Tang's model[13] are closer to the test curve in Fig. 8(c). The fitting curve of Xie's model[15−17] is significantly higher than the experimental curve in the post-peak softening stage, which can't describe the rapid drop of the shear stress at the post-peak.

To further illustrate the fitting accuracy and reliability of Eq. (13), Tang's model[13] and Xie's model[15−17], the determination coefficient R^2 is used and listed in Table 3. For these three types of shear stress−displacement curves of rock joints, it can be seen that the determination coefficient R^2 of Eq. (13) is the largest in the Table 3, indicating that Eq. (13) has a better fitting effect on the direct shear test data and can be better describe the shear stress−displacement curve of rock joint at the pre-peak linear stage, pre-peak yield stage, and post-peak softening stage.

Table 3 R^2 in formula (13), Xie's model[15−17] and Tang's model[13]

Sample No.	R^2		
	Eq.(13)	Xie's model	Tang's model
S1	0.993	0.981	0.991
S6	0.989	0.971	0.984
S11	0.991	0.872	0.989

In addition, the piecewise Eq. (14) in Tang's model[13] shows the shear stress (i.e. residual shear strength) is different at the softening stage and the residual stage at the residual displacement u_r. The model function is discontinuous, which does not conform to the actual shear deformation of rock joints.

The Eq.(13), Tang's model[13] and Xie's model[15−17] are applied to obtain the parameters such as shear stiffness, yield strength, peak strength and residual strength, and the actual value of the test curve is applied to calculate the parameters. If there is no direct shear test of a rough joint rock under a certain normal stress condition, the calculation curve can't be obtained. By carrying out direct shear tests to obtain the shear stress−displacement curve of the rock joint under a certain normal stress, only the model parameters of this specific roughness joint under this normal stress can be determined. All these parameters can only be used to describe the shear deformation behavior of this specific specimen, while the shear deformation behavior

of roughness joints under other normal stresses cannot be described. When all these models are implemented into numerical simulators, it is impossible to simulate the shear deformation behavior of rock joints with different roughness under different normal stresses by inputting the direct shear test parameters of these specific specimens. Therefore, the above models cannot be used as the constitutive model, and the above parameters are required to be further determined. The shear deformation behavior of joints with different roughness under different normal stresses can be described by inputting the model parameters.

4 Constitutive model

4.1 Peak shear stress

The peak shear stress of rock joints can be estimated by Barton's equation[23], and the specific expression is

$$\tau_{\mathrm{p}}=\sigma_{\mathrm{n}}\tan\left[\varphi_{\mathrm{b}}+\mathrm{JRC}\lg\left(\frac{\mathrm{JCS}}{\sigma_{\mathrm{n}}}\right)\right] \tag{17}$$

For fresh un-weathered rock joints, JCS is equal to compressive strength σ_{c}.

Figure 9 shows the predicted peak shear stresses calculated from Eq. (17) and experimental values. It can be seen from Fig. 9 that the data points are distributed around the straight line $y=x$, indicating that the prediction result of Eq. (17) is better, and the predicted value is relatively close to the experimental value.

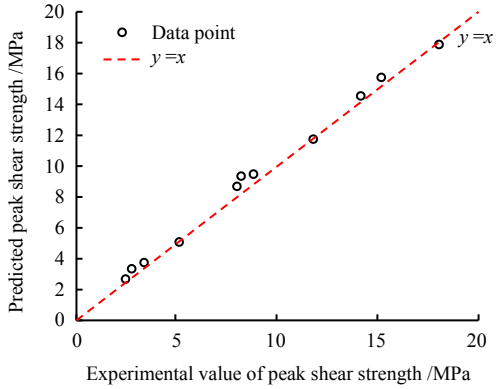

Fig. 9 Comparison of predicted and experimental peak shear stress

In order to quantitatively analyze the prediction accuracy of Eq. (17), the mean value of the relative error is written as

$$\delta=\frac{1}{j}\sum_{i=1}^{j}\left|\frac{M-C}{M}\right| \tag{18}$$

where δ is the mean value of relative error (%); M is the test value of the i-th group of direct shear test (MPa); C is the predicted value of the i-th group of direct shear test (MPa); and j is the serial number of test data sets, respectively.

The calculated mean value of the relative error is 6.9%, which shows that the prediction error of the peak shear stress in Eq. (17) is relatively small, and this formula can be used to estimate the peak shear stress.

4.2 Peak shear displacement

Based on the positive correlation between the peak shear displacement of the joint and the normal stress, and the negative correlation of peak shear displacement with the roughness of the joint, Xia et al.[32] proposed the expression of the peak shear displacement of the regular tooth-shaped joint:

$$\frac{u_{\mathrm{p}}}{L}=a_1\mathrm{e}^{b_1\left(\frac{\sigma_{\mathrm{n}}}{\mathrm{JCS}}\right)\cos i_1} \tag{19}$$

where a_1 and b_1 are fitting parameters; i_1 is the undulation angle; and L is the length of the jointed specimen along the shear direction.

In order to extend Eq. (19) to the irregular joints, the following assumptions are made.

(1) The area of the irregular joint profile is regarded as S_1 and the projection area is regarded as S_2. The angle i_{a} between the two planes can be regarded as the equivalent dilatancy angle of the irregular joint[37], as shown in Fig. 10.

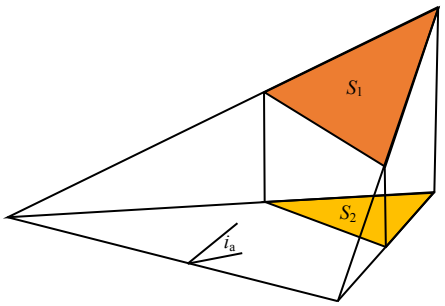

Fig. 10 Calculation model diagram of average climbing angle i_{a}

According to the geometric relationship, the equivalent dilatancy angle i_{a} is calculated as

$$i_{\mathrm{a}}=\arccos\left(1/R_{\mathrm{s}}\right) \tag{20}$$

The calculation equation of the area ratio R_{s} of the profile is

$$R_{\mathrm{s}}=\frac{A_{\mathrm{t}}}{A} \tag{21}$$

where A_{t} is the unfolded area of the profile at the joint surface; and A is the projected area of the joint surface.

(2) The inclination angle of regular joints is regarded as the equivalent dilatancy angle of irregular joints.

$$i_1=i_{\mathrm{a}} \tag{22}$$

Combining Eqs. (19), (20) and (22), the peak shear

displacement of irregular joints is written as

$$u_{\mathrm{p}} = La_1 \mathrm{e}^{b_1\left(\frac{\sigma_{\mathrm{n}}}{\mathrm{JCS}}\right)\frac{1}{R_{\mathrm{s}}}} \tag{23}$$

Based on the direct shear tests, the parameters a_1=0.029 and b_1=3.191 can be calculated by fitting.

Figure 11 shows the joint peak shear displacement test value and the predicted value calculated from Eq. (23). It can be seen from Fig. 11 that the data points are all distributed around the straight line $y=x$, indicating that the prediction result of Eq. (23) is better. The predicted value is closer to the experimental value, and the average relative error is 6.4%. It proves that the Eq. (23) is applicable for the prediction of the peak shear displacement of irregular joints under different normal stresses.

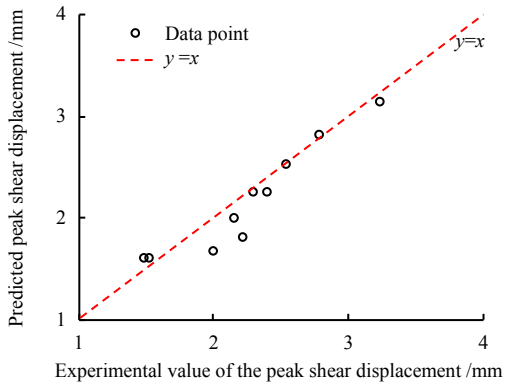

Fig. 11 Comparison of predicted and experimental values of peak shear displacement

4.3 Shear stiffness at the pre-peak stage

The pre-peak shear stiffness is the slope of the fitted straight line in the pre-peak linear stage. The starting and ending points of the linear phase before the peak can be determined by the shear stress difference method proposed by Xie et al. (2020)[17]. The parameters u_1/u_{p}, $u_{\mathrm{y}}/u_{\mathrm{p}}$, τ_1/τ_{p}, and $\tau_{\mathrm{y}}/\tau_{\mathrm{p}}$ under different normal stresses are shown in Fig. 12. They basically fluctuate within a certain range, showing no obvious relationship with the normal stress. Table 4 lists the maximum, minimum and average values of the 4 datasets.

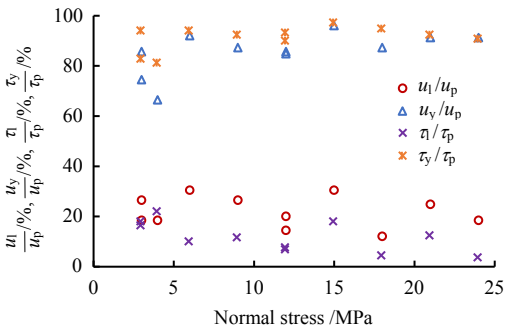

Fig. 12 Relationship between u_1/u_{p}, $u_{\mathrm{y}}/u_{\mathrm{p}}$, τ_1/τ_{p}, $\tau_{\mathrm{y}}/\tau_{\mathrm{p}}$ and normal stress

Table 4 The maximum, minimum and average values of four groups of data

Name	$\frac{u_1}{u_{\mathrm{p}}}$ /%	$\frac{u_{\mathrm{y}}}{u_{\mathrm{p}}}$ /%	$\frac{\tau_1}{\tau_{\mathrm{p}}}$ /%	$\frac{\tau_{\mathrm{y}}}{\tau_{\mathrm{p}}}$ /%
Minimum value	12.3	66.8	3.30	81.1
Maximum value	30.0	96.4	21.3	97.3
Mean value	21.7	85.5	11.4	91.2

It can be seen from Table 4 that the yield shear stress is about 81.1%−97.3% of the peak shear stress, with an average value of 91.2%, which is basically consistent with about 90% of the peak shear stress provided by Hungr et al.(1978)[38]. Goodman[39] found that the yield shear stress was approximately equal to 70%−90% of the peak shear stress. Compared with the values listed in Table 4, this value is about 10% lower.

Here, the mean values of u_1/u_{p}, $u_{\mathrm{y}}/u_{\mathrm{p}}$, τ_1/τ_{p} and $\tau_{\mathrm{y}}/\tau_{\mathrm{p}}$ are used to establish u_1, u_{y}, τ_1 and τ_{y}.

$$\left.\begin{aligned} u_1 &= 0.217u_{\mathrm{p}};\quad u_{\mathrm{y}} = 0.855u_{\mathrm{p}} \\ \tau_1 &= 0.114\tau_{\mathrm{p}};\quad \tau_{\mathrm{y}} = 0.912\tau_{\mathrm{p}} \end{aligned}\right\} \tag{24}$$

Then the pre-peak shear stiffness is written as

$$k_{\mathrm{s}} = \frac{\tau_{\mathrm{y}} - \tau_1}{u_{\mathrm{y}} - u_1} = \frac{0.912\tau_{\mathrm{p}} - 0.114\tau_{\mathrm{p}}}{0.855u_{\mathrm{p}} - 0.217u_{\mathrm{p}}} = 1.251\frac{\tau_{\mathrm{p}}}{u_{\mathrm{p}}} \tag{25}$$

The Eq. (25) is determined by the test values of τ_{p} and u_{p}, and it cannot be used for the prediction of pre-peak shear stiffness. However, the predicted τ_{p} and u_{p} calculated from Eqs. (17) and (23) are substituted into Eq. (25) to calculate the pre-peak shear stiffness, which will result in a certain prediction error. Therefore, the Eq. (25) is corrected as

$$k_{\mathrm{s}} = 1.251q\frac{\tau_{\mathrm{pc}}}{u_{\mathrm{pc}}} \tag{26}$$

where q is the correction factor, and q=0.936 by fitting; τ_{pc} is the predicted value calculated by Eq. (17); and u_{pc} is the predicted value calculated by Eq. (23).

Figure 13 shows the experimental and the predicted values of the pre-peak shear stiffness calculated by Eq. (26). It can be seen from Fig. 13 that the data points

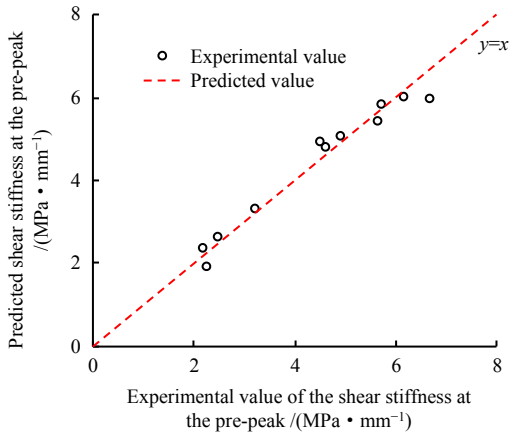

Fig. 13 Comparison of predicted and experimental values of shear stiffness at the pre-peak period

are all distributed around the straight line $y=x$, which shows that the Eq. (26) has a good prediction results, and the mean value of the relative error is 6.3%. This equation can be applied to estimate the pre-peak shear stiffness.

4.4 Fitting parameters of n, t, m, and τ_r

Figures14(a)−14(d) show the relationship between the parameters n, t, m, τ_r and the normal stress.

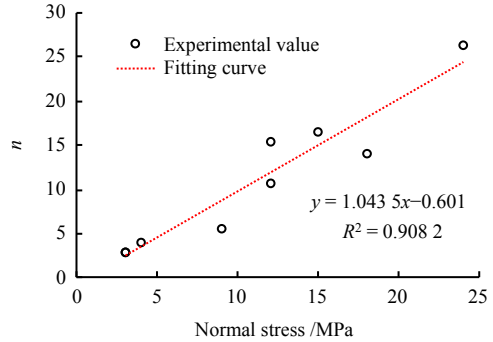

(a) Relationship of parameter n and normal stress

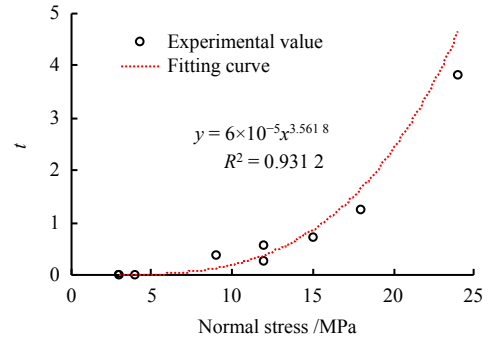

(b) Relationship of parameter t and normal stress

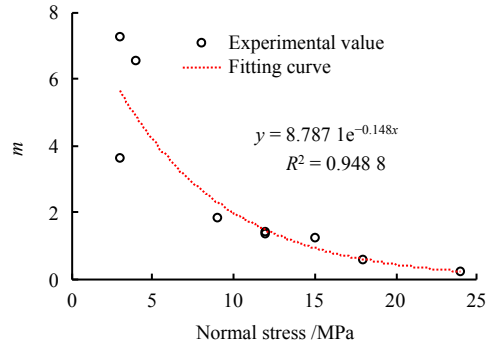

(c) Relationship of parameter m and normal stress

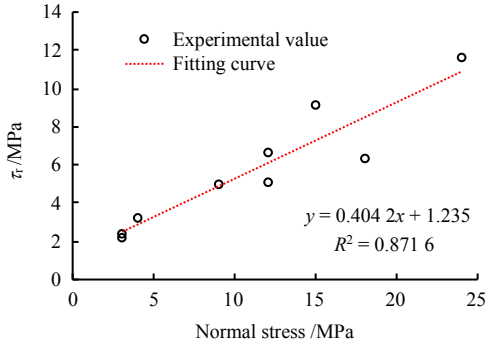

(d) Relationship of parameter τ_r and normal stress

Fig. 14 Relationships between parameters n, t, m, τ_r and normal stress

It can be seen from Fig.14 that the parameters n and τ_r increase linearly with the normal stress, while the parameter t increases in a power function, and the parameter m decreases in an exponential function. Then the expressions of the parameters n, t, m, and τ_r can be written as follows:

$$n = 1.043\ 5\sigma_n - 0.601 \tag{27}$$

$$t = 6\times10^{-5}\sigma_n^{3.561\ 8} \tag{28}$$

$$m = 8.878\ 1\exp(-0.148\sigma_n) \tag{29}$$

$$\tau_r = 0.404\ 2\sigma_n + 1.235 \tag{30}$$

4.5 Prediction of the shear stress−displacement curve of rock joints

As described in Sections 4.1−4.4, the parameters k_s, u_y, u_p, τ_y, τ_p, τ_r, n, t, and m in Eq. (13) can be estimated by the equations considering the basic physical and mechanical parameters of rock joints and experimental condition parameters (e.g., normal stress). Therefore, the shear stress−displacement of rock joints with different roughness can be predicted under different normal stresses after determining the constant of the expression. Meanwhile, the Eq. (13) can be used as the constitutive model of shear deformation of rock joints. In order to verify the correctness of the method, the specimens S1, S6 and S11 are taken as examples to predict the shear stress−displacement curve of rock joints. The detailed prediction steps are as follows.

At first, the shear tests of rock joints with the certain roughness under different normal stresses are carried out, combined with the basic physical and mechanical parameters of rock joints, the functions of parameters k_s, u_y, u_p, τ_y, τ_p, τ_r, n, t, and m are determined. They are then substituted into Eq.(13), which is the shear deformation constitutive model of rock joint. Finally, the shear stress under different shear displacements was calculated by the constitutive model as shown in Fig. 15. The calculated curves of specimens S1, S6, and S11 are close to the experimental curves, with the fitting correlation coefficients of 0.939, 0.946, and 0.908. After including the cumulative errors of the model parameter expressions, the calculation results are still acceptable. The Eq.(13) can be implemented in the numerical simulation software to capture the shear deformation behavior of rock joints.

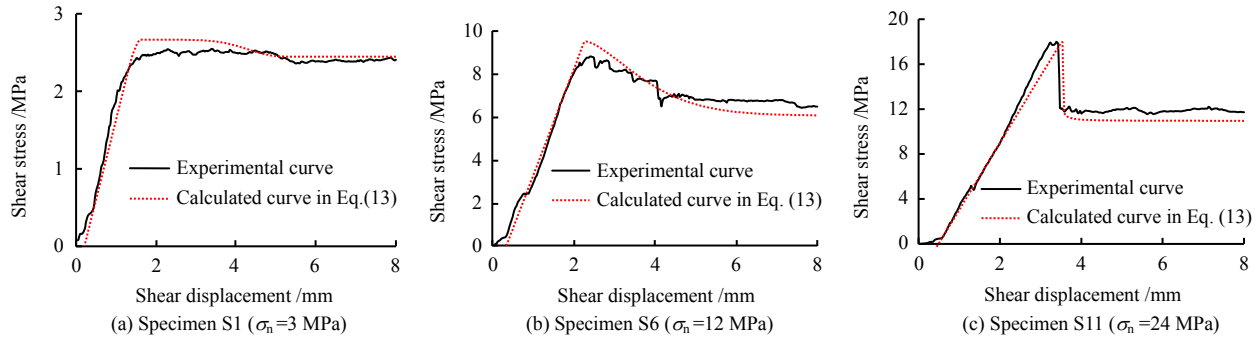

Fig. 15 Comparison of calculated and experimental shear stress−shear displacement curves for different rock specimens

5 Conclusions

(1) Obvious stages can be identified in shear stress−displacement curve of rock joints. Ignoring the pre-peak compaction stage, the shear deformation process of rock joints can be divided into three stages: the pre-peak linear stage, pre-peak yield stage, and the post-peak softening stage. Among them, the decreasing amplitude and rate of shear stress in the post-peak softening stage increase with the increase of normal stress. Thus, the shear stress−displacement curve can be divided into three types: plateau after peak, slow drop after peak, and rapid drop after peak.

(2) According to the shape characteristics of the shear stress−displacement curve of rock joints at each stage, the characteristic parameter expressions of the shear stress−displacement curve are determined and the constitutive model of the shear deformation of rock joints is proposed. By fitting the experimental data, the correctness of the constitutive model is verified. Compared with the Xie's model[15−17] and the Tang's model[13], the new proposed model in this paper has a higher fitting accuracy to the test data, and it is more accurate in describing the shear stress−displacement curve of the rock joints at each stage.

(3) In the proposed shear deformation constitutive model of rock joints, the parameters k_s, u_y, u_p, τ_y, τ_p, τ_r, n, t, and m can be estimated by the basic physical and mechanical parameters of rock joints and test conditions (e.g., normal stress). The shear stress−displacement curve of rock joints with different roughness under different normal stresses can be predicted, which is helpful for the numerical analysis and engineering estimation of the stability of the jointed rock mass.

References

[1] GOODMAN R E, TAYLOR R L, BREKKE T L. A model for the mechanics of jointed rock[J]. Journal of the Soil Mechanics and Foundations Division, 1968, 94(SM3): 638−659.

[2] GOODMAN R E. Methods of geological engineering in discontinuous rocks[M]. New York: West Publishing Company, 1976: 472−490.

[3] BANDIS S C, LUMSDEN A C, BARTON N R. Fundamentals of rock joint deformation[J]. International Journal of Rock Mechanics and Mining Sciences and Geomechanics Abstracts, 1983, 20(6): 249−268.

[4] DESAI C S, FISHMAN K L. Plasticity-based constitutive model with associated testing for joints[J]. International Journal of Rock Mechanics and Mining Sciences & Geomechanics Abstracts, 1991, 28(1): 15−26.

[5] SAEB S, AMADEI B. Modeling rock joints under shear and normal loading[J]. International Journal of Rock Mechanics and Mining Sciences & Geomechanics Abstracts, 1992, 29(3): 267−278.

[6] TANG Zhi-cheng, XIA Cai-chu, XIAO Su-guang. Constitutive model for joint shear stress-displacement and analysis of dilation[J]. Chinese Journal of Rock Mechanics and Engineering, 2011, 30(5): 917−925.

[7] ZHOU Hui, CHENG Gong-tan, ZHU Yong, et al. Experimental study of shear deformation characteristics of marble dentate joints[J]. Rock and Soil Mechanics, 2019, 40(3): 852−860.

[8] AMADEI B, WIBOWO J, STURE S, et al. Applicability of existing models to predict the behavior of replicas of natural fractures of welded tuff under different boundary conditions[J]. Geotechnical and Geology Engineering, 1998, 16(2): 79−128.

[9] SIMON R. Analysis of fault-slip mechanics in hard rock mining[D]. Montreal: McGill University, 1999: 118−120.

[10] GRASSELLIA G, EGGER P. Constitutive law for the shear strength of rock joints based on three-dimensional surface parameters[J]. International Journal of Rock Mechanics and Mining Sciences, 2003, 40(1): 25−40.

[11] SHEN Ming-rong, ZHANG Qing-zhao. Experimental study of shear deformation characteristics of rock mass discontinuities[J]. Chinese Journal of Rock Mechanics and Engineering, 2010, 29(4): 713−719.

[12] XU Lei, REN Qing-wen. A new constitutive model for rock discontinuities[J]. Rock and Soil Mechanics, 2011, 32(Suppl. 1): 217−224.

[13] TANG Zhi-cheng, XIA Cai-chu, DING Zeng-zhi.

Analysis of shear deformation law for intermittent jointed rock mass[J]. Rock and Soil Mechanics, 2011, 32(8): 2353−2358.

[14] TANG Zhi-cheng, XIA Cai-chu, HUANG Ji-hui, et al. Postpeak normalized displacement softening model for discontinuous rock joint[J]. Rock and Soil Mechanics, 2011, 32(7): 2013−2016.

[15] XIE S J, LIN H, WANG Y X, et al. A statistical damage constitutive model considering whole joint shear deformation[J]. International Journal of Damage Mechanics, 2020, 29(6): 988−1008.

[16] XIE S J, LIN H, CHEN Y F, et al. A damage constitutive model for shear behavior of joints based on determination of the yield point[J]. International Journal of Rock Mechanics and Mining Sciences, 2020, 128: 104269.

[17] XIE S J, LIN H, WANG Y X, et al. Nonlinear shear constitutive model for peak shear-type joints based on improved Harris damage function[J]. Archives of Civil and Mechanical Engineering, 2020, DIO: 10.1007/s43452-020-00097-z.

[18] LIN H, XIE S J, YONG R, et al. An empirical statistical constitutive relationship for rock joint shearing considering scale effect[J]. Comptes Rendus Mecanique, 2019, 347(8): 561−575.

[19] NASSIR M, SETTARI A, WAN R. Joint stiffness and deformation behaviour of discontinuous rock[J]. Journal of Canadian Petroleum Technology, 2010, 49(9): 78−86.

[20] KULHAWY F H. Stress deformation properties of rock and rock discontinuities[J]. Engineering Geology, 1975, 9(4): 327−350.

[21] QI Jian-dong, JIN Ai-bing, WANG He, et al. Correction and application of the Bandis empirical formula[J]. Journal of University of Science and Technology Beijing, 2014, 36(12): 1575−1582.

[22] PATTON F D. Multiple modes of shear failure in rock[C]//Proceedings of the 1st Congress of International Society of Rock Mechanics. Lisbon: [s. n.], 1966: 509−513.

[23] BARTON N. Review of a new shear-strength criterion for rock joints[J]. Engineering Geology, 1973, 7(4): 287−332.

[24] GRASSELLI G, WIRTH J, EGGER P. Quantitative three-dimensional description of a rough surface and parameter evolution with shearing[J]. International Journal of Rock Mechanics and Mining Sciences, 2002, 39(6): 789−800.

[25] XIA C C, TANG Z C, XIAO W M, et al. New peak shear strength criterion of rock joints based on quantified surface description[J]. Rock Mechanics and Rock Engineering，2014, 47(2): 387−400.

[26] JIN Lei-lei, WEI Yu-feng, HUANG Xin, et al. Shear strength calculation model of rock joints based on three-dimensional morphology of joint surface[J]. Rock and Soil Mechanics, 2020, 41(10): 3355−3364.

[27] FAN Xiang, DENG Zhi-ying, CUI Zhi-meng, et al. A new peak shear strength model for soft-hard joint[J]. Rock and Soil Mechanics, 2020, 42(7): 1861−1870.

[28] BARTON N, CHOUBEY V. The shear strength of rock joints in theory and practice[J]. Rock Mechanics, 1977, 10(1): 1−54.

[29] WIBOWO J. Effect of boundary conditions and surface damage on the shear behavior of rock joints: tests and analytical predictions[D]. Boulder: University of Colorado at Boulder, 1994.

[30] BARTON N. Modeling rock joint behavior from in-situ block tests: implications for nuclear waste repository design[R]. Columbus: Office of Nuclear Waste Isolation, 1982.

[31] ASADOLLAHI P, TONON F. Constitutive model for rock fractures: revisiting Barton's empirical model[J]. Engineering Geology, 2010, 113(1−4): 11−32.

[32] XIA Cai-chu, TANG Zhi-cheng, SONG Ying-long, et al. Analysis of relationship between joint peak shear displacement and its influence factors[J]. Rock and Soil Mechanics, 2011, 32(6): 1654−1658.

[33] BAN Li-ren, QI Cheng-zhi, SHAN Ren-liang, et al. Pre-peak shear constitutive model considering the softening shear stiffness and its influencing factors[J]. Journal of China Coal Society, 2018, 43(10): 2765−2772.

[34] GUO Bao-hua, CHENG Tan, CHEN Yan, et al. Seepage characteristic of marble fracture and effect of filling sands[J]. Journal of Hydraulic Engineering, 2019, 50(4): 463−-474.

[35] LI C C, ZHANG N, RUIZ J. Measurement of the basic friction angle of planar rock discontinuities with three rock cores[J]. Bulletin of Engineering Geology and the Environment, 2019, 78(2): 847−856.

[36] LI Y, ZHANG Y. Quantitative estimation of joint roughness coefficient using statistical parameters[J]. International Journal of Rock Mechanics & Mining Sciences, 2015, 77: 27−35.

[37] DONG Hang-yu. Experimental study on mechanical shear properties of irregular rock fractures[D]. Jiaozuo: Henan Polytechnic University, 2017.

[38] HUNGR O, COATES D F. Deformability of joints and its relation to rock foundation settlements[J]. Canadian Geotechnical Journal, 1978, 15(2): 239−249.

[39] GOODMAN R E. The deformability of joints[C]// Determination of the In-situ Modulus of Deformation of Rock. West Conshohocken: ASTM International, 1970: 174−196.